PNAS RESEARCH ARTICLE | NEUROSCIENCE OPEN ACCESS

Postsynaptic receptors regulate presynaptic transmitter stability through transsynaptic bridges

Swetha K. Godavarthi[a,b,1], Masaki Hiramoto[c], Yuri Ignatyev[d], Jacqueline B. Levin[e], Hui-quan Li[a,b], Marta Pratelli[a,b], Jennifer Borchardt[f], Cynthia Czajkowski[f], Laura N. Borodinsky[e], Lora Sweeney[d], Hollis T. Cline[c], and Nicholas C. Spitzer[a,b,1]

Contributed by Nicholas C. Spitzer; received October 17, 2023; accepted February 27, 2024; reviewed by Steven J. Burden, Alan D. Grinnell, and U. Jack McMahan

Stable matching of neurotransmitters with their receptors is fundamental to synapse function and reliable communication in neural circuits. Presynaptic neurotransmitters regulate the stabilization of postsynaptic transmitter receptors. Whether postsynaptic receptors regulate stabilization of presynaptic transmitters has received less attention. Here, we show that blockade of endogenous postsynaptic acetylcholine receptors (AChR) at the neuromuscular junction destabilizes the cholinergic phenotype in motor neurons and stabilizes an earlier, developmentally transient glutamatergic phenotype. Further, expression of exogenous postsynaptic gamma-aminobutyric acid type A receptors ($GABA_A$ receptors) in muscle cells stabilizes an earlier, developmentally transient GABAergic motor neuron phenotype. Both AChR and $GABA_A$ receptors are linked to presynaptic neurons through transsynaptic bridges. Knockdown of specific components of these transsynaptic bridges prevents stabilization of the cholinergic or GABAergic phenotypes. Bidirectional communication can enforce a match between transmitter and receptor and ensure the fidelity of synaptic transmission. Our findings suggest a potential role of dysfunctional transmitter receptors in neurological disorders that involve the loss of the presynaptic transmitter.

transmitter receptors | neurotransmitters | transmitter stability | transmitter selection | transsynaptic bridges

Postsynaptic cells differentiate morphologically in response to presynaptic signals. For example, filopodia on the dendrites of cultured mouse hippocampal pyramidal neurons respond to release of glutamate from developing axons, leading to physiological and morphological maturation (1). Dendrites of mouse cortical pyramidal neurons in acute brain slices respond to extracellularly uncaged glutamate or GABA by forming spines that express glutamate or GABA receptors (2, 3). Muscle cells respond to the release of agrin from motor neurons by clustering AChR (4). Cultured skeletal muscle cells respond to cultured glutamatergic neurons by forming functional glutamatergic synapses (5). Also, when neurotransmitters switch, the postsynaptic cells respond to the newly expressed transmitter by expressing a matching receptor (6–9). Conversely, presynaptic cells respond to retrograde signaling by endocannabinoids and neurotrophins, which regulate many functions in the nervous system (10, 11). During synapse development, retrograde signaling by postsynaptic neurotransmitter receptors regulates presynaptic neurotransmitter identity (12). It is unclear whether retrograde signaling regulates neurotransmitter stabilization after synapses have been established.

Glutamate and GABA are transiently expressed in *Xenopus* motor neurons at neural plate and early neural tube stages (13). Following formation of the neuromuscular junction, motor neurons lose these neurotransmitters and the cholinergic phenotype appears (13–15). In loss-of-function and gain-of-function experiments, we took advantage of the presence of the canonical transmitter, acetylcholine (ACh), and the earlier transient expression of glutamate and GABA during development to address the role of postsynaptic receptors in transmitter stabilization. We demonstrate that retrograde signaling by postsynaptic transmitter receptors is necessary and sufficient to stabilize expression of their cognate transmitter in presynaptic motor neurons and that this retrograde signaling is blocked by disruption of receptor-specific transsynaptic bridges.

Results

Blocking Endogenous AChR at the Neuromuscular Junction. We first tested whether blockade of AChR at cholinergic neuromuscular junctions in *Xenopus* larvae affects the expression of ACh in motor neurons. To achieve local unilateral inhibition of AChR, we implanted 120 µm diameter agarose beads containing AChR antagonists, pancuronium or curare, or saline into developing mesoderm at 19 hours postfertilization (hpf) for drug

Significance

Sites of presynaptic neurotransmitter release are tightly correlated with the postsynaptic expression of cognate neurotransmitter receptors. At the same time, many neurons express more than one neurotransmitter and their synaptic partners express more than one population of transmitter receptors. It is essential for information transfer at synapses that transmitters and receptors are matched. Failure to achieve a transmitter–receptor match would cause failure of synaptic transmission. Using pharmacological, immunocytochemical, neurophysiological, and molecular methods, we show that postsynaptic neurotransmitter receptors are necessary and sufficient to achieve the stabilization of their cognate neurotransmitter in the presynaptic neuron. This retrograde signal from different receptors is mediated by physical bridges of proteins involving synapse adhesion molecules. These transsynaptic bridges specify neurotransmitter identity.

Preprint: A version of the manuscript is deposited as a preprint at bioRxiv (https://doi.org/10.1101/2022.09.10.507343).

The authors declare no competing interest.

[1]To whom correspondence may be addressed. Email: skgodavarthi@ucsd.edu or nspitzer@ucsd.edu.

This article contains supporting information online at https://www.pnas.org/lookup/suppl/doi:10.1073/pnas.2318041121/-/DCSupplemental.

Published April 3, 2024.

delivery by diffusion (6, 9, 13) (Fig. 1*A*). We immunostained wholemounts of larvae for choline acetyltransferase (ChAT), the enzyme that synthesizes ACh, and for synaptic vesicle protein 2 (SV2), a marker of nerve terminals, to determine the capacity for ACh synthesis in nerve terminals in the myocommatal junctions at the boundaries between chevrons of myocytes. We then compared the percentage labeled area of ChAT-stained nerve terminals adjacent to pancuronium beads to the percentage labeled area of ChAT-stained terminals adjacent to saline beads in sibling larvae (Fig. 1 *B–E*, *Left*). We also compared the SV2-stained percentage labeled area of the same nerve terminals adjacent to pancuronium beads to SV2-stained percentage labeled area of the same nerve terminals adjacent to saline beads (Fig. 1 *B–E*, *Right*). At 2 days postfertilization (dpf), the areas of ChAT and SV2 staining in larvae with beads containing pancuronium were not different from the staining in saline bead controls and larvae not implanted with beads (Fig. 1 *B* and *E* and *SI Appendix*, Fig. S1*A*). Unaltered SV2 and ChAT expression at 2 dpf suggests that pancuronium beads have not affected assembly of the neuromuscular junctions. Neuromuscular junctions have been assembled by 1 dpf, but not before, as evidenced by the presence of cholinergic mEPPs (miniature end plate potentials) and EPPs in myocytes (14, 15) and confirmed in recordings from larvae at this age (*SI Appendix*, Fig. S2 *A–D*). By 3 dpf, the percentage labeled area of ChAT-stained nerve terminals adjacent to pancuronium beads decreased to 19% of saline controls with no change in staining for SV2 (Fig. 1 *C* and *E* and *SI Appendix*, Fig. S3). Because loading of a transmitter into synaptic vesicles by transporter proteins is an essential component of a transmitter phenotype, we examined the expression of VACHT, the vesicular ACh transporter. Staining for VACHT was reduced to 40% of saline controls at 3 dpf, with no change in staining for SV2 (*SI Appendix*, Fig. S1*B*). By 4 dpf, the staining for ChAT had fallen to 5% of saline controls in response to either pancuronium or curare (Fig. 1 *D* and *E* and *SI Appendix*, Fig. S1 *C* and *D*), while SV2 staining was 73% of saline controls (Fig. 1*E* and Dataset S1). Reduction of SV2 staining likely reflects withdrawal of nerve terminals (16, 17). We observed similar loss of ChAT staining when beads contained 5 μM pancuronium (*SI Appendix*, Fig. S3), a concentration which blocks only postsynaptic myocyte AChR and spares presynaptic neuronal AChR (18). These results suggest that the loss of ChAT precedes the loss of SV2 and show that blockade of postsynaptic AChR impairs the stability of ChAT expression.

Normally, embryonic *Xenopus* motor neurons express glutamate in their cell bodies at 1 dpf (13), which can potentiate ACh release at nerve terminals (19). The level of glutamate decreases by 2 dpf as ChAT begins to be detected (13), and by 3 dpf, glutamate is no longer observed immunohistochemically in most neurons (13). Blockade of AChR with pancuronium led to increased expression of a vesicular glutamate transporter (VGLUT1) in motor neuron terminals at 4 dpf (Fig. 1*F*), suggesting the stabilization of a glutamatergic phenotype. The expression of VGLUT1 in motor neuron terminals was accompanied by a corresponding increase in expression of glutamatergic AMPA and NMDA receptor subunits in myocytes adjacent to these terminals (Fig. 1 *G* and *H*), with staining patterns similar to those observed at earlier stages of development (6). Intracellular recordings from these myocytes at 4 dpf, when beads have lost most or all of their pancuronium, yielded two classes of mEPPs, characterized by blockade by different antagonists, rise and decay times, and frequencies (Fig. 1 *I–K* and *O–Q*). The overall mean frequency was 0.57 ± 0.07 s^{-1}. Rapid-rise rapid-decay mEPPs with a mean frequency of 0.47 ± 0.07 s^{-1} were blocked by NBQX, indicating that they depended on AMPA receptors. The mEPPs remaining after the NBQX block had slower rise and decay times typical of AChR, a mean frequency of 0.07 ± 0.00 s^{-1} and were blocked by the additional application of pancuronium. mEPPs in control larvae implanted with a saline bead had a mean frequency of 1.03 ± 0.07 s^{-1} and were blocked by pancuronium (Fig. 1 *L–M* and *R*). Because quantal content is proportional to mEPP frequency (20, 21), the higher frequency of glutamatergic mEPPs than cholinergic mEPPs may indicate larger evoked glutamate release in response to ACh receptor blockade, which is a feature of homeostatic presynaptic scaling (22, 23). The local block of AChR did not result in immunostaining for GABA in motor neuron terminals (*SI Appendix*, Fig. S1*E*), in agreement with earlier reports that the number of neurons expressing glutamate, but not GABA or glycine, increases following a reduction in neuronal activity (6, 24). These results show that local block of ACh receptors leads to stabilization of expression and function of another excitatory transmitter, glutamate, consistent with the inhibitory effect of ACh on glutamate signaling in CNS neurons (25).

Expressing Exogenous GABA Receptors in Embryonic Myocytes. Embryonic *Xenopus* motor neurons express GABA as well as glutamate in their cell bodies (13) and in their axons (Fig. 2*A*). Ordinarily, the level of GABA decreases by 2 dpf as ChAT appears. We expressed $GABA_A$ receptors in a small number of embryonic myocytes (26) to determine whether these receptors would stabilize expression of GABA in the motor neurons that innervate them. We coinjected the transcripts for rat $GABA_A$ receptor α1-EGFP, β2, and γ2 subunits into the ventral blastomeres (V2) at the eight-cell stage to achieve assembly of $GABA_A$αβγ receptors. Injection of α1-EGFP transcripts alone served as control since expression in this case is restricted to the cytoplasm and does not appear in the plasma membrane (27) (*SI Appendix*, Fig. S4 *A–E*). The EGFP-tag (hence, GFP) on the α1 subunit labeled the transfected myocytes. $GABA_A$αβγ receptors were first reliably detected on the surface of myocytes at 27 hpf (*SI Appendix*, Fig. S5 *A–C*) by fluorescence of BODIPY™ TMR-X-conjugated muscimol, a $GABA_A$ receptor agonist. As noted above, neuromuscular junctions have already formed.

At 1 dpf, the presence of $GABA_A$αβγ receptors had not altered GABA expression at neuromuscular junctions because the expression of GABA in motor neuron axons contacting $GABA_A$αβγ receptor–expressing myocytes was not different from that in motor neuron axons contacting either $GABA_A$α-expressing myocytes or myocytes in larvae that had not been injected with transcripts (Fig. 2 *A–D* and *E–H*). At 2 dpf, the normally decreasing expression of GABA in motor neuron axons was selectively stabilized when they contacted myocytes expressing $GABA_A$αβγ receptors (Fig. 2 *I–L* and *M–P*). Strikingly, at 3 dpf, expression of $GABA_A$αβγ receptors in myocytes led to expression of GABA, VGAT, and GAD65/67 in the nerve terminals that innervate them (Fig. 3 *A–M*). The expression of GABA in motor neuron axons in these embryos was increased specifically in axons contacting myocytes that express $GABA_A$αβγ receptors. Myocytes expressing $GABA_A$α alone did not elicit additional axonal GABA expression (Fig. 3*N*), suggesting that GABA was stabilized by the presence of the cognate postsynaptic receptor. Examination of 20 $GABA_A$αβγ receptor–expressing 3 dpf larvae showed no preferential distribution of GFP-expressing myocytes contacted by GABA-expressing axon terminals along the anterior–posterior axis of the trunk of the larvae (*SI Appendix*, Fig. S6).

ChAT was coexpressed with GABA and VGAT, suggesting that the terminals are processes of motor neurons (*SI Appendix*, Fig. S4 *F–L*). Further support that the nerve terminals expressing GABA and VGAT are from motor neurons came when we traced GABA-labeled axons in the myotome back to spinal cord cell bodies

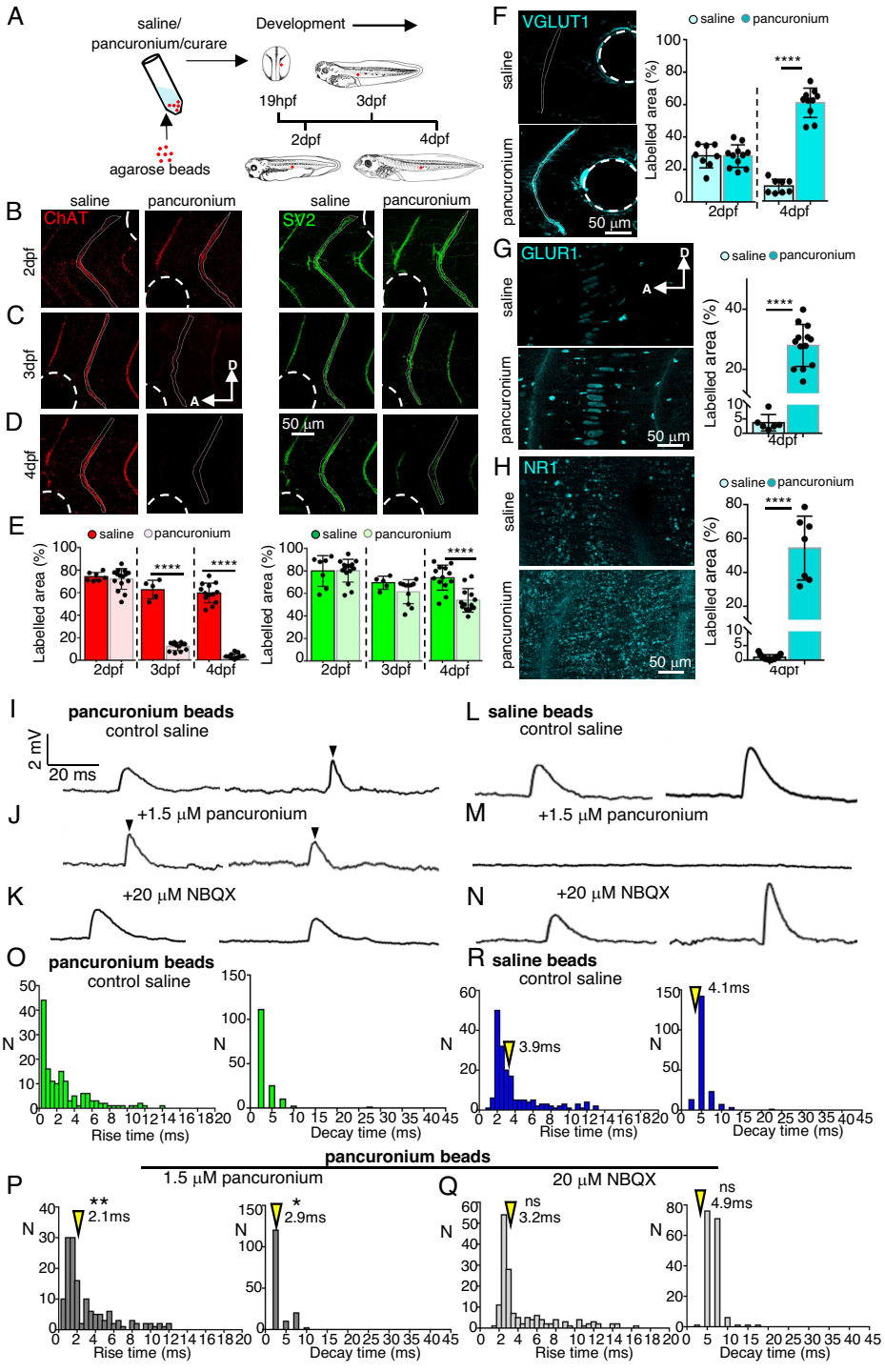

Fig. 1. Local block of AChR in myocytes reduces ChAT expression in motor neuron axons and induces a glutamatergic phenotype. (*A*) Experimental design. A single agarose bead loaded with pancuronium, curare, or saline was implanted into the *Xenopus* mesoderm at 19 hpf. (*B–D*) Wholemounts of bead-implanted larvae (lateral view) were stained at 2 dpf, 3 dpf, and 4 dpf for ChAT and SV2. Dotted lines outline the regions of myocommatal junctions (1/larva) analyzed for quantification of the staining area. Dashed circles indicate positions of beads. (*E*) Area of expression (labeled area above threshold) quantified for ChAT and SV2. n ≥ 5 larvae. (*F–H*) Expression and quantification of VGLUT1, GLUR1, and NR1 in the 4dpf myotome (lateral view) of control and pancuronium-loaded agarose bead-implanted larvae. n ≥ 8 larvae. A, anterior; D, dorsal. (*I–K*) Recordings from pancuronium bead–implanted larvae reveal rapid rise and rapid decay AMPAR-mediated PSP-like mEPPs (arrowheads) that are pancuronium-resistant and NBQX-sensitive, as well as pancuronium-sensitive and NBQX-resistant mEPPs with rise and decay times similar to those described for nicotinic receptor-mediated-mEPPs. (*L–N*) Recordings from saline bead–implanted larvae reveal only pancuronium-sensitive mEPPs. (*O–R*) Rise and decay time distributions for mEPPs in myocytes of pancuronium bead–implanted larvae and saline bead–implanted larvae. N, number of mEPPs. >155 mEPPs (≥3 larvae, 4 dpf) for each group. Only mEPPs with decay times fit by single exponentials were included. Resting potentials were held near −60 mV. Arrowheads indicate median values. The Kolmogorov–Smirnov test compared rise time and decay time in *R* with respective rise and decay time in (*P*) and (*Q*). **P* < 0.05, ***P* < 0.01, *****P* < 0.0001, ns not significant, unpaired two-tailed *t* test. See also *SI Appendix*, Figs. S1–S3 and Dataset S1.

that consistently expressed motor neuron transcription factor Hb9 (*SI Appendix*, Fig. S7). This conclusion was strengthened by the observation that GAD67 and ChAT, as well as GABA and Hb9, are coexpressed in neuronal cell bodies (*SI Appendix*, Fig. S4 *M–P*). Moreover, neurons expressing ChAT and GABA in their cell bodies expressed the Lim3 and not the rAldh1a2 transcription factor. This result demonstrated that these were medial motor neurons produced during the primary wave of neurogenesis (28) and not the lateral motor neurons that are generated later (29) (*SI Appendix*, Fig. S8 *A–D*). Expression of $GABA_A\alpha\beta\gamma$ receptors stabilized the GABAergic phenotype but did not stabilize expression of VGLUT1 or glycine in innervating axons (*SI Appendix*, Fig. S4 *Q–T*).

The stabilization of GABA in axons innervating $GABA_A\alpha\beta\gamma$ receptor–expressing myocytes persisted up to 7 dpf (*SI Appendix*, Fig. S8*E*). To further test whether $GABA_A\alpha\beta\gamma$ receptor–expressing myocytes were specific in stabilizing the presynaptic GABAergic phenotype, we removed mesoderm of 15 hpf uninjected embryos and transplanted into these hosts 15 hpf mesoderm grafts from embryos expressing $GABA_A\alpha\beta\gamma$ receptors or $GABA_A\alpha$ alone. SV2-stained axons that contacted $GABA_A\alpha\beta\gamma$ receptor myocytes in the grafts expressed ChAT and GABA; axons that contacted $GABA_A\alpha$-expressing myocytes expressed only ChAT (Fig. 4 *A–F* and Dataset S2). Thus, stabilization of GABA in axons depended on the $GABA_A\alpha\beta\gamma$ receptor myocytes and not on GABA expression within the spinal cord.

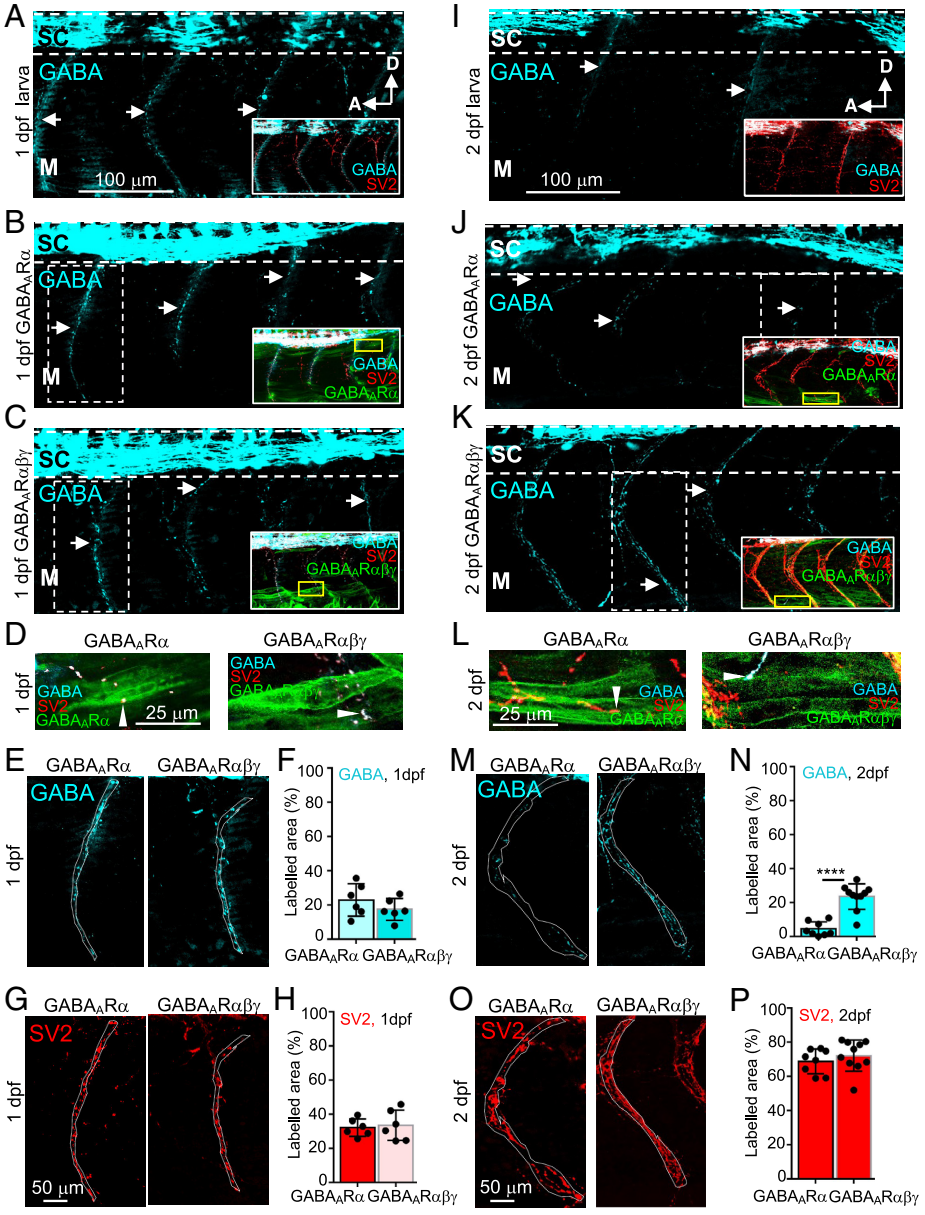

Fig. 2. GABA$_A$Rαβγ expression in myocytes does not affect GABA expression in motor neuron axons contacting these myocytes at 1dpf but increases GABA expression at 2 dpf. (*A* and *B*) 1 dpf axonal GABA expression in the myotome of a normal larva and a GABA$_A$Rα larva. Arrows identify myocommatal junctions. (*C*) 1 dpf GABA expression in the myocommatal junctions of a GABA$_A$Rαβγ larva is not different from that in the GABA$_A$Rα larva. (*A–C*, *Insets*) GABA, SV2 or GABA, SV2 and GABA$_A$R expression in myocytes. (*D*, *Left*) magnified GABA+SV2+ process from the GABA$_A$Rα larva contacts GFP+ myocytes (arrowhead and area indicated by yellow box in *B*). (*Right*) magnified GABA+SV2+ processes from GABA$_A$Rαβγ larva contact GFP+ myocytes (arrowhead and area indicated by yellow box in *C*). (*E–H*) Magnified myocommatal junctions from dashed boxes in *B* and *C*. Quantification of 1 dpf expression of GABA and SV2. Dotted lines outline regions of myocommatal junctions analyzed. n = 6 larvae. (*I* and *J*) 2 dpf axonal GABA expression in the myotome of a normal larva and a GABA$_A$Rα larva have decreased compared to GABA expression at 1 dpf (*A* and *B*). (*K*) 2 dpf GABA expression in the myotome of a GABA$_A$Rαβγ larva is greater than in the GABA$_A$Rα larva. (*I–K*, *Insets*) GABA, SV2 or GABA, SV2 and GABA$_A$R expression in myocytes. (*L*, *Left*) magnified GABA-SV2+ process from the GABA$_A$Rα larva contacts a GFP+ myocyte (arrowhead and area indicated by yellow box in *J*). (*Right*) magnified GABA+SV2+ process from the GABA$_A$Rαβγ larva contacts a GFP+ myocyte (arrowhead and area indicated by yellow box in *K*). (*M–P*) Magnified myocommatal junctions from dashed boxes in *J* and *K*. Quantification of 2 dpf expression of GABA and SV2. n ≥ 8 larvae. Five-fold increase in the 2dpf GABA-labeled area of motor neuron axons contacting GABA$_A$Rαβγ-expressing myocytes relative to GABA$_A$Rα-expressing myocytes (*N* and *K* versus *J*), with no difference in SV2-labeled area of motor neuron axons (*P*), indicates stabilization of GABA expression in axons contacting GABA$_A$Rαβγ-expressing myocytes. Dotted lines outline regions of myocommatal junctions analyzed. ****P < 0.0001 using two-tailed t test. A, anterior; D, dorsal. SC, spinal cord. M, myotome. See also *SI Appendix*, Figs. S4 and S5.

To assess the functional consequence of anatomical innervation by nerve terminals expressing both ChAT and GABA, we recorded mEPPs from GABA$_A$αβγ receptor–expressing myocytes at 4 dpf. We observed two classes of mEPPs, distinguished on the basis of their blockade by different antagonists, their rise and decay times, and their mean frequency (6), with an overall frequency of 0.79 ± 0.07 s^{-1}. Those with faster times occurred at a frequency of 0.57 ± 0.03 s^{-1} and were blocked by pancuronium, showing that they depended on AChR. Those with slower times occurred at a frequency of 0.24 ± 0.04 s^{-1} and were blocked by bicuculline (Fig. 5 *A–C* and *G–I*), indicating that they depended on GABA$_A$αβγ receptors. In contrast, only a single class of mEPPs at a frequency of 0.98 ± 0.13 s^{-1} was observed when recording from myocytes that expressed GABA$_A$α alone. These mEPPs had rise and decay times similar to mEPPs recorded from GABA$_A$αβγ receptor–expressing myocytes in the presence of bicuculline (Fig. 5 *D–F* and *J*). The results of these recordings demonstrate that GABA can be functionally released from motor nerve terminals and innervate myocytes that express GABA$_A$αβγ receptors.

Signal Transduction by Transsynaptic Bridges. We then considered the possible role of transsynaptic bridges in regulating the stability of presynaptic GABA and ACh (30–32). Presynaptic neurexins and postsynaptic neuroligins and dystroglycans are synaptic adhesion molecules that are important for proper maturation and function of synaptic contacts (33). They bridge the synaptic cleft and create a potential pathway for retrograde signaling. However, in heterologous synapse formation assays with neuroligin 1 and neurexin 1β, neuroligin 1 induced both a glutamatergic and a GABAergic phenotype at the same time (34). To determine whether transsynaptic bridges could regulate cholinergic stability versus GABAergic stability at the neuromuscular junction, we tested the role of postsynaptic receptor-specific auxiliary subunits and associated proteins, which are components of endogenous transsynaptic bridges. The GABA$_A$αβγ receptor auxiliary subunit GARLH4 mediates the interaction between the γ subunit of the GABA$_A$αβγ receptor and neuroligin 2, which binds to neurexin (35). A clue was provided by the finding that expression of α and β transcripts of the GABA$_A$ receptor resulted in surface expression of receptors with channel properties similar to those

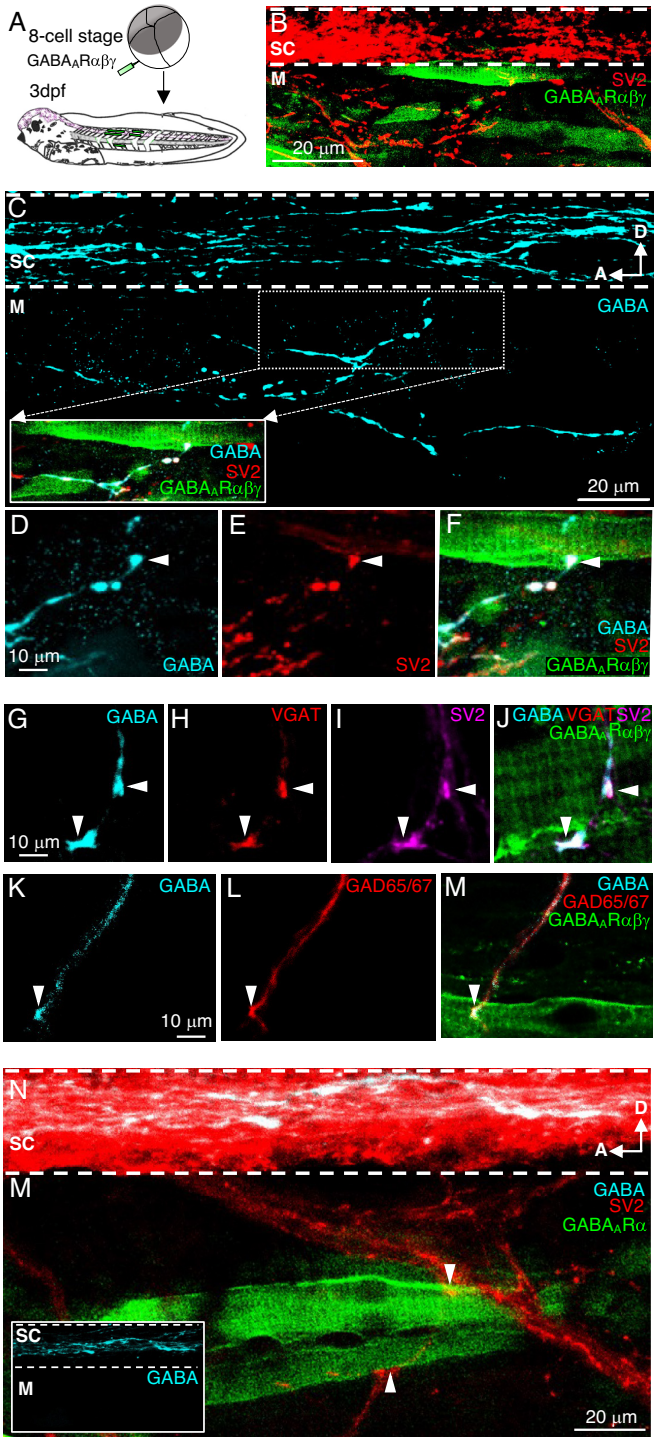

Fig. 3. GABA$_A$Rαβγ expression in myocytes leads to GABA expression in axons that contact them. (*A*) Injection of ventral blastomeres (V2) with GABA$_A$Rαβγ mRNA at the eight-cell stage results in myocyte-specific GABA$_A$R expression. (*B*) Expression of GABA$_A$Rαβγ in sparse myocytes. SV2 labels axons in the spinal cord and in the trunk myotome. (*C*) In an expansion of the field of view in (*B*), staining for GABA reveals GABA+ axons in the spinal cord and coursing ventrally and posteriorly over the trunk myotome. (*Inset*) GFP+ myocyte contacted by the GABA+SV2+ axon from the dotted box. (*D–F*) Higher magnification of contact in (*C*) (arrowheads). (*B–F*) n = 13 larvae. (*G–J*) A GABA+VGAT+SV2+ axon contacts a different GABA$_A$Rαβγ myocyte. n = 6 larvae. (*K–M*) A GABA+GAD65/67+ axon contacts another GABA$_A$Rαβγ myocyte. n = 10 larvae. (*N*) Injection of ventral blastomeres (V2) with GABA$_A$Rα mRNA results in sparse expression of GABA$_A$Rα in myocytes. SV2+ axons contact a GABA$_A$Rα-expressing GFP+ myocyte (arrowheads). n = 7 larvae. (*Inset*) GABA+ axons are restricted to the spinal cord. M, trunk myotome; SC, spinal cord; A, anterior; D, dorsal. All larvae 3 dpf. See also *SI Appendix*, Figs. S4–S8 and Dataset S2.

of GABA$_A$αβγ receptors (27). We found that none of the 12 GABA$_A$αβ receptor–expressing larvae expressed GABA in motor neuron axons that contacted GFP-labeled myocytes, and in all these cases, GABA expression remained restricted to the spinal cord (*SI Appendix*, Fig. S9 and Dataset S2). This result suggested that the presence of the GABA$_A$ receptor γ subunit of the GABA$_A$αβγ receptor might be required for a transsynaptic bridge to stabilize the presynaptic GABAergic phenotype.

To investigate directly whether transsynaptic bridges stabilize presynaptic transmitters, we first used pan-neurexin and pan-neuroligin antibodies to confirm the presence of neurexin (36) and neuroligin at the *Xenopus* neuromuscular junction of larvae expressing GABA$_A$ receptor transcripts (*SI Appendix*, Fig. S10 *A* and *B*). The presence of α-dystroglycan was previously established (37). We ascertained that GARLH4 is expressed in the myocommatal junctions of GABA$_A$αβγ receptor–expressing larvae (*SI Appendix*, Fig. S10 *C–F*) and that the postsynaptic AChR complex-associated protein Lrp4 (38, 39) is expressed in the myocommatal junctions of wild-type larvae (*SI Appendix*, Fig. S10 *G–J*). We then injected morpholinos into the V2 blastomeres at the eight-cell stage to knock down GARLH4 in myocytes and disrupt regulation by GARLH4–neuroligin–neurexin transsynaptic bridges (Fig. 6 *A–C* and *F* and *SI Appendix*, Figs. S10 *C–F* and S11). This experiment prevented the GABA$_A$αβγ receptor-mediated stabilization of GABA in motor neurons (Fig. 6 *D*, *E*, *G*, and *H* and *SI Appendix*, Fig. S12 *A–C*) but did not alter ChAT expression (*SI Appendix*, Fig. S13 *A* and *C* and *D*). These results indicated that GARLH4 is necessary for the expression of presynaptic GABA and implicated regulation by transsynaptic bridges. Similarly, we injected morpholinos into the V2 blastomeres to knock down Lrp4 (38, 39) in myocytes and disrupt regulation by AChR-rapsyn-Lrp4-MuSK-dystroglycan-neurexin transsynaptic bridges (40, 41) (Fig. 6 *I–K* and *SI Appendix*, Figs. S10 *G–J* and S11). This experiment recapitulated the destabilization and loss of ChAT that we observed in the presence of pancuronium (Fig. 6 *L–Q*), without affecting the ability of GABA$_A$αβγ receptors to induce GABA in the motor neurons *SI Appendix*, Fig. S13 *B*, *D*, and *E* and Dataset S3). These results suggested that Lrp4 is required for expression of presynaptic ChAT and pointed to regulation by transsynaptic bridges.

Larvae in which Lrp4 was knocked down exhibited two classes of mEPPs at 4 dpf, differing in their blockade by different antagonists, their rise and decay times (*SI Appendix*, Fig. S14 *A–C* and *G–I*), and their mean frequency, with an overall frequency of 0.63 ± 0.15 s^{-1}. Pancuronium-resistant NBQX-sensitive glutamatergic mEPPs had a frequency of 0.53 ± 0.16 s^{-1}. Pancuronium-sensitive, NBQX-resistant cholinergic mEPPs had a frequency of 0.05 ± 0.01 s^{-1}. These cholinergic mEPPs, for which there were also fewer AChR (42), were smaller in amplitude compared to cholinergic mEPPs in larvae expressing the control morpholino (1.7 ± 0.1 mV versus 2.7 ± 0.1 mV; $n^{mEPP} = 177$, $N^{larvae} = 7$; $P < 0.0001$, two-tailed *t* test). mEPPs in control larvae implanted with a saline bead occurred at a frequency of 1.20 ± 0.09 s^{-1} and were blocked by pancuronium (*SI Appendix*, Fig. S14 *D–F* and *J*). The effect of knocking down Lrp4 may be phenocopied by pancuronium through binding to the α and γ subunits of the AChR (43) and altering the AChR-Lrp4 interaction, thereby disrupting signaling through cholinergic transsynaptic bridges.

We next considered CASK (Ca^{2+}/calmodulin-activated Ser-Thr kinase) as a candidate that could receive signals from the presynaptic ends of the transsynaptic bridges and stabilize transmitter expression in the motor neurons. CASK is a membrane-associated guanylate kinase (44) and transcription factor that binds to neurexin protein

presynaptically (Fig. 7*A*) and is present at both glutamatergic (45) and GABAergic (46) synapses. CASK pre-mRNA is subject to alternative splicing that yields proteins with preferences to interact with many targets (47). Autophosphorylated CASK translocates to the nucleus and induces transcription of genes essential for development (48, 49). Additionally, neurexin-1 competes as a CASK phosphorylation substrate, preventing CASK autophosphorylation (50). The splice variants, together with differential phosphorylation, identified CASK as a potentially significant player in stabilizing presynaptic expression of different neurotransmitters. We found that CASK is expressed in the myocommatal junctions and spinal cord of normal *Xenopus* larvae (*SI Appendix*, Fig. S10 *K–O*). Knocking down presynaptic CASK, by injecting morpholinos into the D1.2 blastomeres at the 16-cell stage to target the spinal cord (51) (Fig. 7 *B–D* and *H* and *SI Appendix*, Figs. S10 *N* and *O* and S11), disrupted both $GABA_A\alpha\beta\gamma$ receptor-mediated GABA stabilization and AChR-mediated ChAT stabilization in motor neurons (Fig. 7 *E–G* and *I–N* and Dataset S3). Knockdown of CASK, Lrp4, or GARLH4 did not alter laminin expression or the extent of labeling by synaptophysin (SYN) (*SI Appendix*, Fig. S15 *A–C*), suggesting that there was no change in the gross morphology of the myocommatal junction or postsynaptic myocytes.

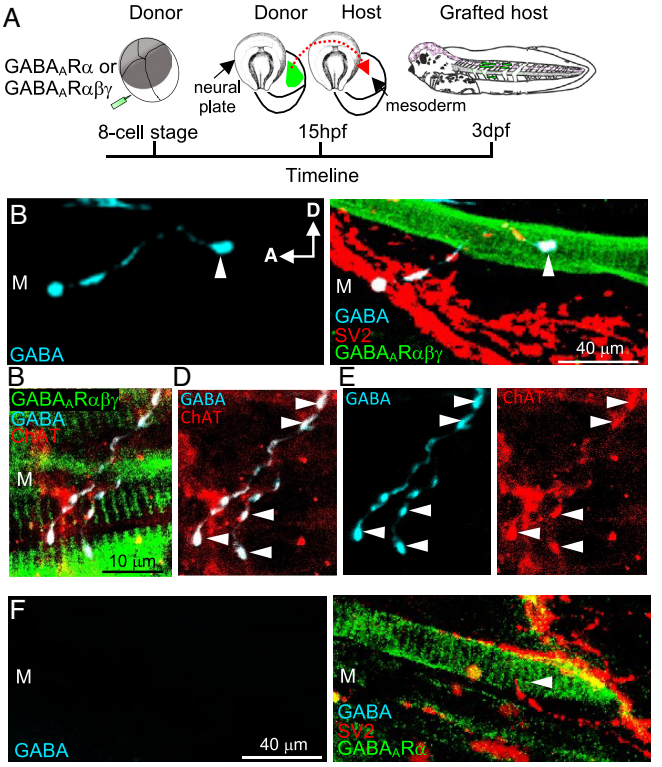

Fig. 4. Grafting $GABA_A R\alpha\beta\gamma$ receptor–expressing mesoderm into host embryos results in $GABA_A R\alpha\beta\gamma$ receptor expression in myocytes and GABA expression in motor neurons contacting these myocytes. (*A*) Procedure for mesodermal transplantation. (*Left* to *Right*) donor *Xenopus* embryo injected at the eight-cell stage with $GABA_A R\alpha$ or $GABA_A R\alpha\beta\gamma$ mRNA in the ventral blastomeres (V2). The neural plate was lifted to access the presomitic mesoderm (green), which was grafted from the donor to wild-type host larva at 15 hpf (red arrow). GFP expression was detected in the myotome of the host larva at 3 dpf. (*B*, *Left*) A GABA+ axon courses ventrally and posteriorly over the trunk myotome (M) in a $GABA_A R\alpha\beta\gamma$-expressing, mesoderm-grafted host. (*Right*) The GABA+SV2+ axon (arrowhead) contacts a $GABA_A R\alpha\beta\gamma$-expressing GFP+ myocyte. (*C*) Another $GABA_A R\alpha\beta\gamma$ myocyte is contacted by a GABA+ChAT+ axon in the trunk myotome (M). (*D*) Isolation of GABA+ChAT+ axons in *C*. (*E*) Individual channels for GABA and ChAT in (*D*). n = 5 larvae. (*F*, *Left*) No GABA is detected in the trunk myotome (M) in $GABA_A R\alpha$-expressing, mesoderm-grafted host. (*Right*) A GABA-SV2+ axon (arrowhead) contacts a $GABA_A R\alpha$-expressing GFP+ myocyte. n = 5 larvae. All larvae 3 dpf. A, anterior; D, dorsal.

Presynaptic localization of CASK in motor neuron nuclei and in myocommatal junctions, however, depended on the integrity of the cholinergic or GABAergic transsynaptic bridge (Fig. 7 *O* and *P*). In control larvae, in the presence of the cholinergic transsynaptic bridge, CASK expression was observed in both the nuclei and the myocommatal junctions. Knocking down Lrp4, to disrupt the cholinergic transsynaptic bridge, reduced CASK expression to 37% of controls in the SYN- labeled myocommatal junctions but did not reduce CASK expression in the Hoechst-labeled nuclei. This result suggests that cytoplasmic expression of CASK in the motor neuron axon or cell body is required to stabilize cholinergic transmission. Expressing $GABA_A\alpha\beta\gamma$ receptors and simultaneously disrupting the cholinergic transsynaptic bridge reduced CASK expression in the nuclei to 26% of controls but did not reduce CASK expression in the SYN-labeled myocommatal junctions. This finding suggests that reduction in nuclear expression of CASK is necessary to stabilize GABAergic transmission. As expected, disrupting the GABAergic transsynaptic bridge in the presence of the cholinergic transsynaptic bridge recapitulated the CASK expression that was observed in control larvae.

Discussion

To address the role of postsynaptic receptors in transmitter stabilization, we took advantage of the presence of the canonical junctional transmitter, ACh, and the early expression of glutamate and GABA as they are disappearing from motor neurons during development. Our results demonstrate that blockade of AChR at the neuromuscular junction destabilizes the cholinergic phenotype in motor neurons and stabilizes an earlier glutamatergic phenotype. Moreover, expression of $GABA_A\alpha\beta\gamma$ receptors stabilizes an earlier GABAergic motor neuron phenotype. Spontaneous mEPPs and EPPs are present prior to the reduction of ChAT expression by pancuronium and prior to enhancement of GABA expression by $GABA_A\alpha\beta\gamma$ receptors, indicating that these manipulations do not alter the initial formation of the synapse. Thus, postsynaptic neurotransmitter receptors regulate the stability of presynaptic neurotransmitters at newly formed neuromuscular junctions.

This regulation is achieved by noncanonical retrograde signaling by postsynaptic receptors (52, 53) that operates through transsynaptic bridges (Fig. 8). The specificity of regulation relies on receptor-specific auxiliary subunits and associated proteins linked to neuroligin and dystroglycan at the postsynaptic end of the GABAergic and cholinergic bridges. When the cholinergic bridge was disrupted by knockdown of Lrp4, ChAT expression was reduced, and glutamate was stabilized. When the $GABA_A\alpha\beta\gamma$ receptor was expressed, GABA expression was stabilized unless GARLH4 was knocked down. For both GABA and ACh, the change in transmitter stability was specific to the perturbation and no change was observed in the stability of the other transmitter. Our results are consistent with a model in which knockdown of Lrp4 or GARLH4, together with knockdown of CASK, knocks down the on-ramp and the off-ramp of the transsynaptic bridges, preventing signal transmission across the synaptic cleft along the bridges formed by neurexins, neuroligins, and dystroglycans (36).

Knockdown of MuSK was not tested, as its absence would prevent assembly of the neuromuscular junction (54). Knockdown of dystroglycan would not distinguish between effects on cholinergic and GABAergic junctions (55–57). Knockdown of neurexin and neuroligin was not tested (58, 59). Our data suggest that neurexin serves as the presynaptic end of both the cholinergic and GABAergic transsynaptic bridges, receiving postsynaptic receptor–dependent signals and transmitting them through the neurexin-interacting protein

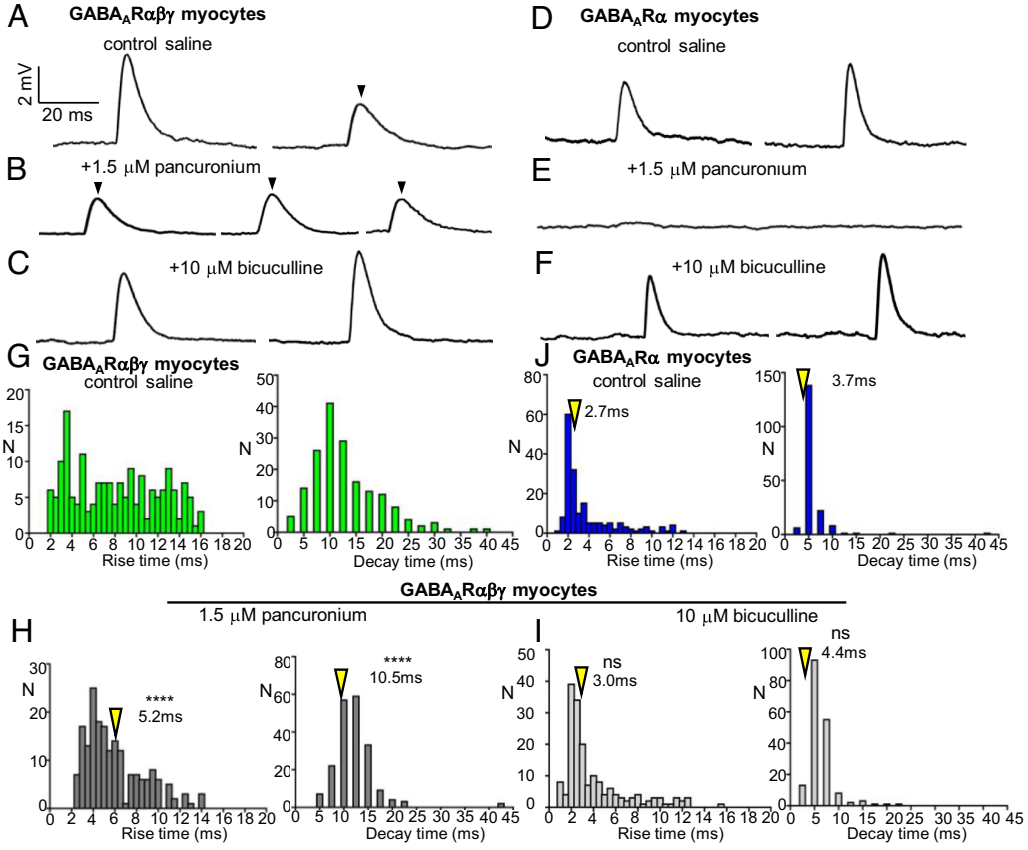

Fig. 5. Neuromuscular junctions of myocytes expressing GABA$_A$Rαβγ generate GABAergic and cholinergic mEPPs. (*A*–*C*) Recordings from GABA$_A$Rαβγ myocytes reveal pancuronium-resistant and bicuculline-sensitive mEPPs (arrowheads; n = 7 larvae), as well as pancuronium-sensitive and bicuculline-resistant mEPPs (n = 7 larvae). (*D*–*F*) Recordings from GABA$_A$Rα myocytes in the presence of saline, pancuronium, and bicuculline reveal only pancuronium-sensitive and bicuculline-resistant mEPPs (n = 5 larvae). (*G*–*I*) Recordings from GABA$_A$Rαβγ myocytes reveal both pancuronium-sensitive, bicuculline-resistant mEPPs with kinetics of nicotinic receptor mEPPs and pancuronium-resistant, bicuculline-sensitive mEPPs with kinetics of GABA$_A$R-mediated mEPPs. (*J*) Recordings from GABA$_A$Rα myocytes in the presence of saline reveal rise and decay time distributions for mEPPs similar to (*I*). N, number of mEPPs. N ≥ 178 mEPPs (n ≥ 5 larvae) for each group. All recordings at 4 dpf. Only mEPPs with decay times fit by single exponentials were included. Resting potentials were held near –60 mV. Arrowheads indicate median values. The Kolmogorov–Smirnov test compared rise time and decay time in *J* with respective rise and decay time in *H* and *I*. ****$P < 0.0001$, ns not significant. See also Dataset S2.

CASK to achieve presynaptic cholinergic or GABAergic stabilization. The receptor-dependent distribution of CASK within the presynaptic neuron, likely coupled with its roles in scaffolding the synapse (60), organizing presynaptic voltage-gated calcium channels (61), and regulating neuronal gene transcription (48), appears to provide a mechanism by which different postsynaptic receptors stabilize cognate neurotransmitter expression. This signaling system of transsynaptic bridges shares features with clustered protocadherin cell adhesion molecules (62), some of which change the nuclear versus cytoplasmic distribution of β-catenin to regulate the Wnt pathway (63).

The appearance of glutamate receptors following AChR blockade and the appearance of glutamatergic mEPPs following either AChR blockade or Lrp4 knockdown, as well as the expression of GABA$_A$αβγ receptors, are linked to a reduction in the frequency of cholinergic mEPPs. Although not tested here, this would likely produce a reduction in the safety factor for transmission (64). The reduced frequencies could arise because of changes in the level of ChAT, competition for a limited pool of synaptic vesicles, changes in vesicle release, or changes in the level or extent of AChR (65). Interestingly, the loss of AChR precedes the loss of nerve terminals in a mouse model of myasthenia gravis (MG) (66). MG is often the result of an autoimmune attack on AChR function (67–69). Our findings suggest that reduced levels of presynaptic ACh, in addition to loss of AChR, may contribute to the muscle fatigue that is observed in MG.

The reduction we observed in presynaptic cholinergic markers upon blockade of postsynaptic ACh receptors is consistent with presynaptic homeostatic plasticity, in which a compensatory increase in neurotransmitter upon loss of receptor function is preceded by a compensatory change in receptor subunits (22, 23, 70–72). In *Xenopus* myocytes, where the AChR block cannot be rescued by alternative subunits (73, 74), reduction in presynaptic ChAT and VACHT was observed. Expression of glutamate receptors in myocytes (6, 75) led to stabilization of presynaptic glutamate (76, 77). Our results are consistent with the effectiveness of alternative, reserve receptor subunits in homeostatic synaptic plasticity at mammalian CNS synapses (78, 79). Our results are also consistent with the observation of a decrease in the *Drosophila* presynaptic active zone protein Bruchpilot, which is associated with presynaptic transmitter synthesis and release (80). Irrespective of differences between some of the molecular components at the *Drosophila* and *Xenopus* neuromuscular junctions, both junctions rely on neurexins and neuroligins and transsynaptic bridges. The decrease in Bruchpilot occurs following the blockade of postsynaptic receptor subunits (81) that occurs early in homeostatic presynaptic scaling (70, 82). The decrease is reversed only when the receptor function is restored by expression and insertion of a different, reserve receptor subunit (70, 71). These findings again link the stability of transmitter expression to the presence of an appropriate postsynaptic receptor.

What is the receptor-specific retrograde signal? Although we have identified one protein, CASK, with receptor-specific presynaptic distribution, the molecular mechanism by which this is achieved remains unknown. Our findings demonstrate the presence of neurexins at *Xenopus* neuromuscular junction. Further investigation will determine whether different isoforms or splice variants of neurexins are recruited to GABAergic and cholinergic transsynaptic bridges or whether a receptor-specific conformational change in neurexin results in differential recruitment or phosphorylation of CASK. Other presynaptic signaling proteins that act independently or along with neurexin and CASK may also contribute to stabilization of the appropriate transmitter. In addition, the demonstration that transsynaptic bridges are involved in transmitter stabilization does not preclude a role for postsynaptic diffusible factors, some of which have been shown to influence synapse formation and maintenance retrogradely

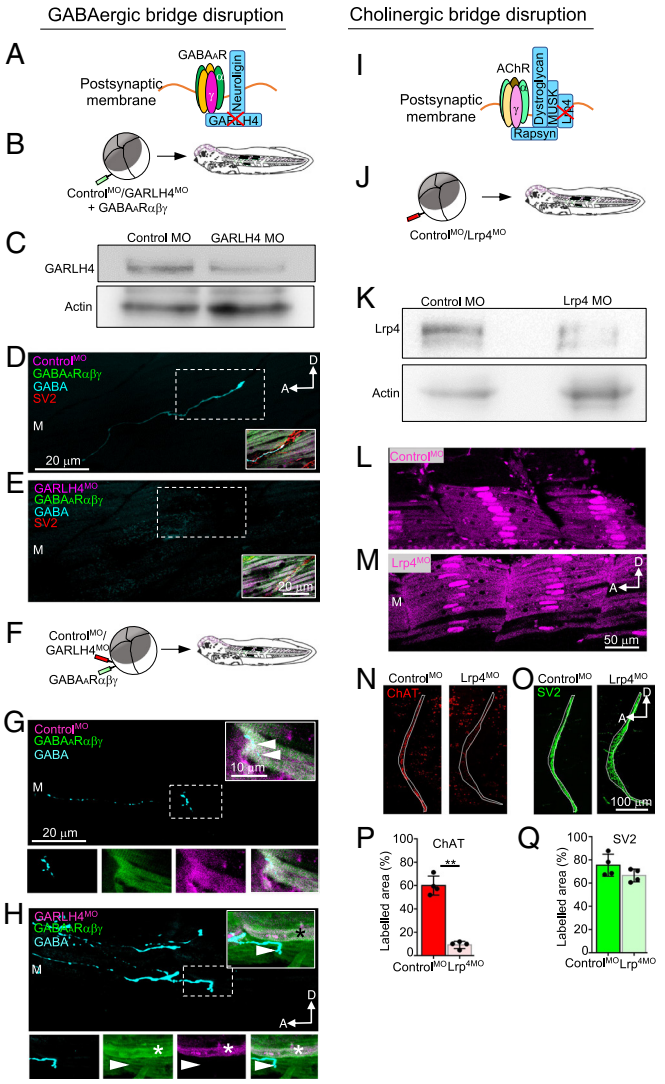

Fig. 6. Knockdown of postsynaptic components of transsynaptic bridges prevents receptor-driven presynaptic neurotransmitter stabilization. (*A*) GARLH4 links $GABA_AR\alpha\beta\gamma$ to neuroligin in the postsynaptic membrane. (*B*) Simultaneous injection of ventral blastomeres (V2) with $GABA_AR\alpha\beta\gamma$ mRNA along with control morpholino (control^{MO}) or GARLH4^{MO} (6 nL of 1 mM MO) to achieve widespread expression of $GABA_AR$ and MOs in myocytes. (*C*) Presence of GARLH4 and morpholino knockdown validation by western blot. (*D*) A GABA+ axon is observed in the myotome of a control^{MO} $GABA_AR\alpha\beta\gamma$ larva (dashed box, GABA channel only, 7/7). (*Inset*) Area in the dashed box. A GABA+SV2+ axon contacts a control^{MO}+GFP+ myocyte. (*E*) No GABA+ axon is observed in the myotome of a GARLH4^{MO} $GABA_AR\alpha\beta\gamma$ larva (dashed box, GABA channel only, 0/12), (*Inset*) Area in the dashed box. An SV2+ axon contacts a GARLH4^{MO}+GFP+ myocyte. n/N, larvae with GABA+ axon/total larvae examined. (*F*) Staggered injection of ventral blastomeres (V2) with $GABA_AR\alpha\beta\gamma$ mRNA followed 1 min later by low dose of control^{MO} or GARLH4^{MO} (3 nL of 1 mM MO) to achieve sparse expression of MOs in myocytes. (*G*) A GABA+ axon is observed in a control^{MO} $GABA_AR\alpha\beta\gamma$ larva (dashed box, GABA channel only, 5/5). (*Inset*) Area in the dashed box. A GABA+ axon contacts a control^{MO}+GFP+ myocyte (arrowheads). (*H*) GABA+ axon observed in the myotome of a GARLH4^{MO}/normal larva (dashed box, GABA channel only, 12/12). (*Inset*) Area in the dashed box. A GABA+ axon contacts a $GABA_AR\alpha\beta\gamma$ myocyte lacking GARLH4^{MO} (arrowhead, 12/12). GABA+ processes were not observed contacting GARLH4^{MO} $GABA_AR\alpha\beta\gamma$ myocytes (e.g., asterisk, 0/12). (*I*) Lrp4 links to the AChR through postsynaptic MuSK, dystroglycan and rapsyn. (*J*) Injection of ventral blastomeres (V2) with a high dose of Lrp4^{MO} or control^{MO} (6 nL of 1 mM MO) to achieve widespread expression of MOs in myocytes. (*K*) Morpholino knockdown validation by western blot. (*L* and *M*) Control^{MO} and Lrp4^{MO} expression in the myotome. (*N* and *O*) Myocommatal junctions of larvae with control or Lrp4^{MO} stained for ChAT and SV2. (*P* and *Q*) Labeled area above threshold quantified for ChAT and SV2. n = 4, $^{**}P = 0.0092$, two-tailed *t* test. Red X in *A* and *G*, proteins knocked down in *B*–*H* and *J*–*Q*. M, myotome; SC, spinal cord; NT, neurotransmitter; A, anterior; D, dorsal. All larvae 3 dpf. See also *SI Appendix*, Figs. S9–S16 and Dataset S3.

(12, 83–86). It will be of interest to determine whether deficits in postsynaptic receptors or transsynaptic bridges contribute to reduced transmitter levels at neuronal synapses in the mature nervous system and to pathological change in neurological disorders.

Neurotransmitter release is closely coupled with the expression of cognate neurotransmitter receptors postsynaptic to the release sites (70, 87). Mechanisms to accomplish this transmitter–receptor match are necessary to produce this precision because neurons can have more than one neurotransmitter and their synaptic partners can express more than one population of transmitter receptors. If a neuron released one transmitter, and the postsynaptic cell expressed receptors for a different transmitter, synaptic transmission would fail. Spatially localized, bidirectional signaling, as described here, can achieve the transmitter–receptor match essential for robust communication in neural circuits.

Methods

Animals. All animal procedures were performed in accordance with institutional guidelines and approved by the UCSD Institutional Animal Care and Use Committee. See *SI Appendix* for further details.

Local Drug Delivery. Spatial and temporal control of delivery of pharmacological agents was achieved using agarose beads (100 to 200 mesh, Bio-Rad) loaded with 2 mM Ca^{2+} medium with or without drugs and implanted at 19 hpf (stage 18) (6, 9, 13). See *SI Appendix* for further details.

Whole-Mount Immunohistochemistry. Whole *Xenopus* larvae were fixed at the indicated stages of development and processed for immunostaining with the following antibodies: ChAT (1:500, Millipore, AB144P), SV2 (1:500, Developmental Studies Hybridoma Bank, AB2315387), VGLUT1 (1:200, Millipore, AB5905), GLUR1 (1:200, MilliporeSigma, MAB2263), NR1 (1:200, MilliporeSigma, MAB363), VAChT (1:500, GenScript, SC 1180-AG), GABA (1:200, Millipore, ABN131), VGAT (1:300, cytoplasmic domain, Synaptic Systems, 131013), GFP (1:500, Synaptic Systems, 132005), GAD65/67 (1:50, Abcam, ab11070), Hb9 (1:10, Developmental Studies Hybridoma Bank, 81.5C10), GAD67 (1:250, Millipore, MAB5406), Glycine (1:200, Millipore, AB139), Lim3 (1:200, Millipore, AB3202), rAldh1a2 (1:8,000, ZMBBI Columbia, CU1022), pan-Neurexin (1:200, kind gift from Peter Scheiffele), pan-Neuroligin (1:200, Invitrogen, PA5-77523), SYN (1:200, Synaptic Systems, 101002), laminin (1:200, MilliporeSigma, L9393), Lrp4 (1:500, extracellular domain, generous gift from Stephan Kröger), GARLH4 (1:200, LifeSpan Biosciences, LS-C170010), and CASK (1:200, Santa Cruz Biotechnology, SC-13158). See *SI Appendix* for further details.

Image Acquisition. Confocal images of whole larvae were acquired with a Leica Stellaris 5 confocal microscope with 25×/0.95 water immersion objective, at a z-resolution of 0.5 mm, and analyzed with FIJI. For the CASK-Hoechst, 4-channel, and 5-channel immunostaining experiments, images of whole larvae were acquired on a Leica SP8 at the UC San Diego School of Medicine microscopy core with 40×/1.30 oil immersion objective at a z-resolution of 0.5 μm. Imaging parameters were kept constant within each developmental stage and set of different protein markers.

Image Analysis. Images were analyzed in FIJI. Percent of labeled area was determined by measuring the fraction occupied by pixels of intensity at or above an empirically determined constant threshold. For GABA receptor expression experiments, larvae were analyzed along the entire A-P axis. To identify GABA+Hb9+ cell bodies in the spinal cord, GABA+ axons were located in the myotome and traced back to the spinal cord using the 3D-Viewer and Simple Neurite Tracing plugins in FIJI. Colocalization of GABA, VGAT, and SV2 was determined for each larva by examining all the optical sections within a confocal stack without maximal projection. FIJI software was used to count fluorescent, immunolabeled ChAT+, Hb9+, Lim3+, GABA+, and GAD67+ cell bodies in the spinal cord; all slices within the confocal stack through the spinal cord were examined without

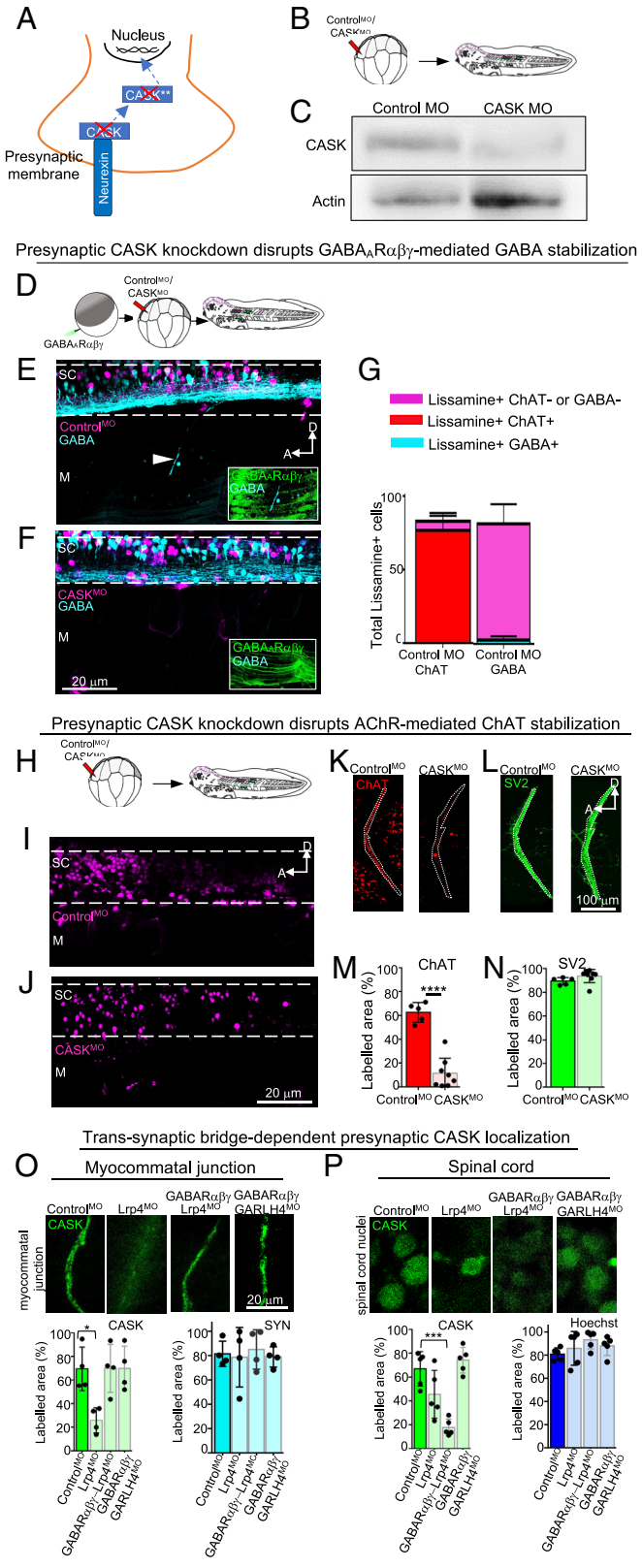

Fig. 7. Knockdown of a presynaptic component of transsynaptic bridges prevents receptor-driven presynaptic neurotransmitter stabilization. (*A*) CASK links to neurexin in the presynaptic membrane. (*B*) Injection of a high dose of CASK^{MO} or control^{MO} (6 nL of 1 mM MO) in dorsal blastomeres 1.2 (D1.2) at the 16-cell stage. All MOs were lissamine-tagged. (*C*) Presence of CASK and morpholino knockdown validation by western blot. (*D*) Injection of GABARαβγ mRNA in ventral blastomeres (V2) to achieve expression in myocytes, and a high dose of CASK^{MO} or control^{MO} (6 nL of 1 mM MO) in dorsal blastomeres 1.2 (D1.2) to achieve widespread transfection of spinal cord cells. (*E*) GABA+ axon in the myotome of control^{MO} GABARαβγ larva (arrowhead, 6/6). (*F*) No GABA+ axons in the myotome of CASK^{MO}GABA$_A$Rαβγ larvae (0/12). (*G*) When the control^{MO} was injected into the dorsal blastomeres 1.2 (D1.2), most lissamine+ somata in spinal cords were ChAT+ (red) (77/83), indicating that the MO transfects motor neurons. When stained for GABA, only a small number of spinal cord lissamine+ somata were GABA+ (cyan) (3/82); the rest were either lissamine+GABA- or lissamine+ChAT- (magenta) (79/82). Total lissamine cells counted per larva ≥71. n = 3. (*H*) Injection of control^{MO} or CASK^{MO} (6 nL of 1 mM MO) in dorsal blastomeres 1.2 (D1.2). (*I*) Larva expressing the control^{MO} in the SC. (*J*) Larva expressing the CASK^{MO} in the SC. (*K* and *L*) Myocommatal junctions of larvae with control^{MO} or CASK^{MO} stained for ChAT and SV2. (*M* and *N*) Labeled area above threshold quantified for ChAT and SV2. n ≥ 5, ****$P < 0.0001$, two-tailed *t* test. (*O* and *P*) Myocommatal junctions of larvae with control^{MO}, Lrp4^{MO}, GABA$_A$Rαβγ-Lrp4^{MO}, or GABA$_A$Rαβγ-GARLH4^{MO} stained for CASK in synaptophysin (SYN)+ motor neuron terminals along the myocommatal junction and in Hoechst+ nuclei in the spinal cord. (*O*) Area of expression of CASK and SYN. n = 4, *$P < 0.01$, one-way ANOVA ($F_{3,12} = 6.316$, $P = 0.0081$). (*P*) Area of expression of CASK and Hoechst. n = 5, ***$P < 0.0001$, one-way ANOVA ($F_{3,12} = 16.5$, $P < 0.0001$). n/N, larvae with GABA+ axon/total larvae observed. Red X in *A*, protein knocked down. M, myotome; SC, spinal cord; A, anterior; D, dorsal. All larvae 3 dpf. See also *SI Appendix*, Figs. S10, S11, S13, S15, and S16 and Dataset S3.

maximal projection. Representative images are maximum intensity projections of five consecutive slices. See *SI Appendix* for further details.

Electrophysiology. Recording techniques and analysis are described in *SI Appendix*.

Plasmids and Morpholinos. Expression of GABA$_A$R was achieved with GABA$_A$R subunit plasmids for α1-EGFP, β2, and γ2 generated in the Czajkowski lab (27). The lissamine-tagged GARLH4, Lrp4, and CASK translation-blocking and splice-blocking morpholinos were supplied by GeneTools (Philomath, OR). See *SI Appendix* for further details.

Microinjections. See *SI Appendix* for further details.

Protein Extraction and ELISA. ELISAs for GFP-tagged GABA$_A$Rα subunit expression in the muscle and spinal cord were performed per the manufacturer's instructions (GFP ELISA Kit, Cell Biolabs). Dissection and sample preparation are described in *SI Appendix*.

Muscimol-BODIPY Staining. Embryos or larvae at the appropriate stages of development (indicated in the Results) were skinned and incubated in 20 mM muscimol-BODIPY [reconstituted in 0.1× MMR (Marc's Modified Ringer's)] for 20 min on an orbital shaker at 22 °C protected from light. Samples were imaged immediately after mounting, for a maximum of 15 min, to ensure that the images were collected during the developmental stages indicated. See *SI Appendix* for further details.

Mesoderm Grafting. Myocyte-dependent stabilization of GABA in innervating motor neuron axons was assessed by mesoderm grafts. To obtain myocyte-specific GABA$_A$Rαβγ or GABA$_A$Rα expression, the presomitic mesoderm of normal embryos 15 hpf (St 13 to 14) was replaced with the presomitic mesoderm explant dissected from sibling embryos expressing either GABA$_A$Rαβγ or GABA$_A$Rα transcripts. The grafting technique was similar to that previously described (88). See *SI Appendix* for further details.

Western Blotting. Protein for western blotting of components of transsynaptic bridges was extracted as described above except that larvae were anesthetized on ice and RIPA lysis buffer was supplemented with phosphatase inhibitors (PhosSTOP, Roche). Protein detection by western blotting was performed for Lrp4 (1:8,000, extracellular domain, generous gift from Stephan Kröger), GARLH4 (1:500, LifeSpan Biosciences, LS-C170010), and CASK (1:500, Santa Cruz Biotechnology, SC-13158). The same blots were reprobed for the loading control actin (1:1,000, Sigma-Aldrich, A2066-100UL). Signal was detected using Clarity ECL Western substrate (BioRad) and imaged on a BioRad ChemiDoc Touch Imaging System. See *SI Appendix* for further details.

Statistics. We used Fisher's exact test for calculating percentage success (presence of GABA+ peripheral axon for GOF studies) in each group (GABA$_A$Rαβγ versus GABA$_A$Rα larvae) for these experiments. All statistical analysis was performed in GraphPad Prism. Values were expressed as mean ± SD. Statistical

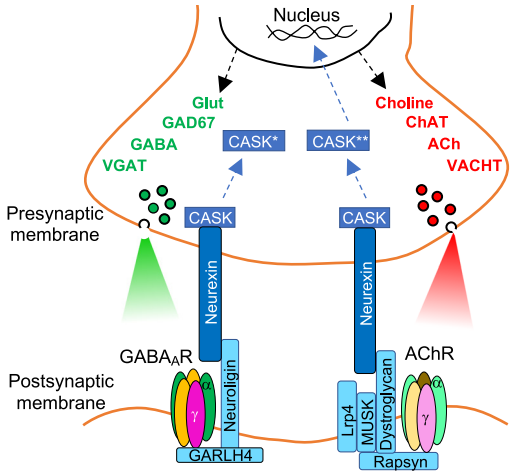

Fig. 8. Model of receptor-driven neurotransmitter stabilization mediated by transsynaptic bridges. Summary of interactions between neurotransmitter receptors and transsynaptic bridge proteins that signal retrogradely to achieve presynaptic transmitter stabilization.

differences were analyzed using the unpaired, two-tailed Student's *t* test or one-way ANOVA or Kolmogorov–Smirnov test. The statistical test used and the *P* values for each measurement are provided in the figure legends and Datasets S1–S3. $P < 0.05$ was considered statistically significant. See *SI Appendix* for further details.

Data, Materials, and Software Availability. All data are included in the manuscript and/or supporting information.

ACKNOWLEDGMENTS. We thank all members of the Spitzer laboratory for discussions and critical feedback; K. Marek for discussions of acknowledgment signals; I. Gregor and R. Aricescu for discussions of receptor pharmacology and transsynaptic bridges; C. Kintner for advice on *Xenopus* blastomere lineage; A. Ray and E. Park for guidance on miniature analysis; A. Glavis-Bloom, S.U. Choi, S. Atkins, M. Gupta, and S. Malladi for technical assistance; and D. K. Berg and L. R. Squire for comments on the manuscript. This work was supported by NSF 2051555 and the Overland Foundation. Microscopy for five-channel imaging utilized the UCSD School of Medicine Microscopy Core, supported by NIH grant NS047101.

Author affiliations: [a]Neurobiology Department, University of California San Diego, La Jolla, CA 92093; [b]Kavli Institute for Brain & Mind, University of California San Diego, La Jolla, CA 92093; [c]Neuroscience Department, The Scripps Research Institute, La Jolla, CA 92037; [d]Institute of Science and Technology Austria, Klosterneuburg 3400, Austria; [e]Department of Physiology & Membrane Biology Shriners Hospital for Children Northern California, University of California Davis School of Medicine, Sacramento, CA 95817; and [f]Neuroscience Department, University of Wisconsin Madison, Madison, WI 53705

Author contributions: S.K.G., M.H., and N.C.S. designed research; S.K.G. and M.H. performed research; S.K.G., M.H., Y.I., J.B.L., H.-q.L., M.P., J.B., C.C., L.N.B., L.S., and H.T.C. contributed new reagents/analytic tools; S.K.G. and N.C.S. analyzed data; N.C.S. secured funding; and S.K.G. and N.C.S. wrote the paper.

Reviewers: S.J.B., MGH/Harvard; A.D.G., David Geffen School of Medicine at UCLA; and U.J.M., Texas A&M University.

1. H. A. Mattison, D. Popovkina, J. P. Y. Kao, S. M. Thompson, The role of glutamate in the morphological and physiological development of dendritic spines. *Eur. J. Neurosci.* **39**, 1761–1770 (2014).
2. H.-B. Kwon, B. L. Sabatini, Glutamate induces de novo growth of functional spines in developing cortex. *Nature* **474**, 100–104 (2011).
3. W. C. Oh, S. Lutzu, P. E. Castillo, H.-B. Kwon, De novo synaptogenesis induced by GABA in the developing mouse cortex. *Science* **353**, 1037–1040 (2016).
4. U. J. McMahan *et al.*, Agrin isoforms and their role in synaptogenesis. *Curr. Opin. Cell Biol.* **4**, 869–874 (1992).
5. M. Ettorre *et al.*, Glutamatergic neurons induce expression of functional glutamatergic synapses in primary myotubes. *PLoS One* **7**, e31451 (2012).
6. L. N. Borodinsky, N. C. Spitzer, Activity-dependent neurotransmitter-receptor matching at the neuromuscular junction. *Proc. Natl. Acad. Sci. U.S.A.* **104**, 335–340 (2007).
7. D. Dulcis, N. C. Spitzer, Illumination controls differentiation of dopamine neurons regulating behaviour. *Nature* **456**, 195–201 (2008).
8. D. Dulcis, P. Jamshidi, S. Leutgeb, N. C. Spitzer, Neurotransmitter switching in the adult brain regulates behavior. *Science* **340**, 449–53 (2013).
9. D. R. Hammond-Weinberger, Y. Wang, A. Glavis-Bloom, N. C. Spitzer, Mechanism for neurotransmitter-receptor matching. *Proc. Natl. Acad. Sci. U.S.A.* **117**, 4368–4374 (2020).
10. P. E. Castillo, T. J. Younts, A. E. Chávez, Y. Hashimotodani, Endocannabinoid signaling and synaptic function. *Neuron* **76**, 70–81 (2012).
11. A. W. Harrington, D. D. Ginty, Long-distance retrograde neurotrophic factor signalling in neurons. *Nat. Rev. Neurosci.* **14**, 177–187 (2013).
12. B. A. Habecker, S. C. Landis, Noradrenergic regulation of cholinergic differentiation. *Science* **264**, 1602–1604 (1994).
13. C. M. Root, N. A. Velázquez-Ulloa, G. C. Monsalve, E. Minakova, N. C. Spitzer, Embryonically expressed GABA and glutamate drive electrical activity regulating neurotransmitter specification. *J. Neurosci.* **28**, 4777–4784 (2008).
14. R. W. Kullberg, T. L. Lentz, M. W. Cohen, Development of the myotomal neuromuscular junction in Xenopus laevis: An electrophysiological and fine-structural study. *Dev. Biol.* **60**, 101–129 (1977).
15. S. Blackshaw, A. Warner, Onset of acetylcholine sensitivity and endplate activity in developing myotome muscles of *Xenopus*. *Nature* **262**, 217–218 (1976).
16. L. M. Murray, L. H. Comley, T. H. Gillingwater, S. H. Parson, The response of neuromuscular junctions to injury is developmentally regulated. *FASEB J.* **25**, 1306–1313 (2011).
17. L. H. Comley *et al.*, Motor unit recovery following Smn restoration in mouse models of spinal muscular atrophy. *Hum. Mol. Genet.* **31**, 3107–3119 (2022).
18. M. Jonsson *et al.*, Distinct pharmacologic properties of neuromuscular blocking agents on human neuronal nicotinic acetylcholine receptors: A possible explanation for the train-of-four fade. *Anesthesiology* **105**, 521–533 (2006).
19. W. M. Fu, J. C. Liou, Y. H. Lee, H. C. Liou, Potentiation of neurotransmitter release by activation of presynaptic glutamate receptors at developing neuromuscular synapses of Xenopus. *J. Physiol.* **489**, 813–823 (1995).
20. M. Kuno, S. A. Turkanis, J. N. Weakly, Correlation between nerve terminal size and transmitter release at the neuromuscular junction of the frog. *J. Physiol.* **213**, 545–556 (1971).
21. A. D. Grinnell, A. A. Herrera, Physiological regulation of synaptic effectiveness at frog neuromuscular junctions. *J. Physiol.* **307**, 301–317 (1980).
22. G. W. Davis, Homeostatic control of neural activity: From Phenomenology to molecular design. *Annu. Rev. Neurosci.* **29**, 307–323 (2006).
23. G. Turrigiano, Homeostatic synaptic plasticity: Local and global mechanisms for stabilizing neuronal function. *Cold Spring Harb. Perspect. Biol.* **4**, a005736 (2012).
24. L. N. Borodinsky *et al.*, Activity-dependent homeostatic specification of transmitter expression in embryonic neurons. *Nature* **429**, 523–530 (2004).
25. T. G. J. Allen, F. C. Abogadie, D. A. Brown, Simultaneous release of glutamate and acetylcholine from single magnocellular "cholinergic" basal forebrain neurons. *J. Neurosci.* **26**, 1588–1595 (2006).
26. S. A. Moody, Fates of the blastomeres of the 16-cell stage *Xenopus* embryo. *Dev. Biol.* **119**, 560–578 (1987).
27. J. X. Connor, A. J. Boileau, C. Czajkowski, A GABA$_A$ receptor α1 subunit tagged with green fluorescent protein requires a β subunit for functional surface expression. *J. Biol. Chem.* **273**, 28906–28911 (1998).
28. A. Lumsden, Neural development: A 'LIM code' for motor neurons? *Curr. Biol.* **5**, 491–495 (1995).
29. L. B. Sweeney *et al.*, Origin and segmental diversity of spinal inhibitory interneurons. *Neuron* **97**, 341–355.e3 (2018).
30. J. Dai, K. Liakath-Ali, S. R. Golf, T. C. Südhof, Distinct neurexin-cerebellin complexes control AMPA- and NMDA-receptor responses in a circuit-dependent manner. *eLife* **11**, e78649 (2022).
31. J. Dai, C. Patzke, K. Liakath-Ali, E. Seigneur, T. C. Südhof, GluD1 is a signal transduction device disguised as an ionotropic receptor. *Nature* **595**, 261–265 (2021).
32. S. P. Gangwar *et al.*, Molecular mechanism of MDGA1: Regulation of neuroligin 2:neurexin trans-synaptic bridges. *Neuron* **94**, 1132–1141.e4 (2017).
33. T. C. Südhof, Synaptic neurexin complexes: A molecular code for the logic of neural circuits. *Cell* **171**, 745–769 (2017).
34. X. Jiang, R. Sando, T. C. Südhof, Multiple signaling pathways are essential for synapse formation induced by synaptic adhesion molecules. *Proc. Natl. Acad. Sci. U.S.A.* **118**, e2000173118 (2021).
35. T. Yamasaki, E. Hoyos-Ramirez, J. S. Martenson, M. Morimoto-Tomita, S. Tomita, Garlh family proteins stabilize GABA$_A$ receptors at synapses. *Neuron* **93**, 1138–1152.e6 (2017).
36. M. S. Sons *et al.*, α-Neurexins are required for efficient transmitter release and synaptic homeostasis at the mouse neuromuscular junction. *Neuroscience* **138**, 433–446 (2006).
37. M. Cohen, C. Jacobson, E. Godfrey, K. Campbell, S. Carbonetto, Distribution of alpha-dystroglycan during embryonic nerve-muscle synaptogenesis. *J. Cell Biol.* **129**, 1093–1101 (1995).
38. N. Yumoto, N. Kim, S. J. Burden, Lrp4 is a retrograde signal for presynaptic differentiation at neuromuscular synapses. *Nature* **489**, 438–442 (2012).
39. N. Kim *et al.*, Lrp4 is a receptor for agrin and forms a complex with musk. *Cell* **135**, 334–342 (2008).
40. E. D. Apel, D. J. Glass, L. M. Moscoso, G. D. Yancopoulos, J. R. Sanes, Rapsyn is required for MuSK signaling and recruits synaptic components to a MuSK-containing scaffold. *Neuron* **18**, 623–635 (1997).
41. A. Barik *et al.*, Lrp4 is critical for neuromuscular junction maintenance. *J. Neurosci.* **34**, 13892–13905 (2014).
42. M. Akaaboune, S. M. Culican, S. G. Turney, J. W. Lichtman, Rapid and reversible effects of activity on acetylcholine receptor density at the neuromuscular junction in vivo. *Science* **286**, 503–507 (1999).
43. D. X. Fu, S. M. Sine, Competitive antagonists bridge the alpha-gamma subunit interface of the acetylcholine receptor through quaternary ammonium-aromatic interactions. *J. Biol. Chem.* **269**, 26152–26157 (1994).
44. K. Tabuchi, T. Biederer, S. Butz, T. C. Südhof, CASK participates in alternative tripartite complexes in which mint 1 competes for binding with caskin 1, a novel CASK-binding protein. *J. Neurosci.* **22**, 4264–4273 (2002).
45. T. C. Südhof, Neuroligins and neurexins link synaptic function to cognitive disease. *Nature* **455**, 903–911 (2008).
46. K. A. Han *et al.*, Lar-rptps directly interact with neurexins to coordinate bidirectional assembly of molecular machineries. *J. Neurosci.* **40**, 8438–8462 (2020).
47. D. Tibbe, Y. E. Pan, C. Reißner, F. L. Harms, H.-J. Kreienkamp, Functional analysis of CASK transcript variants expressed in human brain. *PLoS One* **16**, e0253223 (2021).

48. Y.-P. Hsueh, T.-F. Wang, F.-C. Yang, M. Sheng, Nuclear translocation and transcription regulation by the membrane-associated guanylate kinase CASK/LIN-2. *Nature* **404**, 298–302 (2000).
49. T.-N. Huang, H.-P. Chang, Y.-P. Hsueh, CASK phosphorylation by PKA regulates the protein–protein interactions of CASK and expression of the NMDAR2b gene. *J. Neurochem.* **112**, 1562–1573 (2010).
50. K. Mukherjee *et al.*, CASK functions as a Mg2+-independent neurexin kinase. *Cell* **133**, 328–339 (2008).
51. S. A. Moody, M. J. Kline, Segregation of fate during cleavage of frog (*Xenopus laevis*) blastomeres. *Anat. Embryol. (Berl.)* **182**, 347–362 (1990).
52. S. Valbuena, J. Lerma, Non-canonical signaling, the hidden life of ligand-gated ion channels. *Neuron* **92**, 316–329 (2016).
53. X. Wang, J. M. McIntosh, M. M. Rich, Muscle nicotinic acetylcholine receptors may mediate trans-synaptic signaling at the mouse neuromuscular junction. *J. Neurosci. Off. J. Soc. Neurosci.* **38**, 1725–1736 (2018).
54. D. J. Glass *et al.*, The receptor tyrosine kinase MuSK is required for neuromuscular junction formation and is a functional receptor for agrin. *Cold Spring Harb. Symp. Quant. Biol.* **61**, 435–444 (1996).
55. S. Lévi *et al.*, Dystroglycan is selectively associated with inhibitory GABAergic synapses but is dispensable for their differentiation. *J. Neurosci.* **22**, 4274–4285 (2002).
56. F. Briatore *et al.*, Dystroglycan mediates clustering of essential GABAergic components in cerebellar purkinje cells. *Front. Mol. Neurosci.* **13**, 164 (2020).
57. J. H. Trotter, C. Y. Wang, P. Zhou, G. Nakahara, T. C. Südhof, A combinatorial code of neurexin-3 alternative splicing controls inhibitory synapses via a trans-synaptic dystroglycan signaling loop. *Nat. Commun.* **14**, 1771 (2023).
58. J. Li, J. Ashley, V. Budnik, M. A. Bhat, Crucial role of Drosophila neurexin in proper active zone apposition to postsynaptic densities, synaptic growth and synaptic transmission. *Neuron* **55**, 741–755 (2007).
59. M. Sun *et al.*, Neuroligin 2 is required for synapse development and function at the *Drosophila* neuromuscular junction. *J. Neurosci.* **31**, 687–699 (2011).
60. S. Butz, M. Okamoto, T. C. Südhof, A tripartite protein complex with the potential to couple synaptic vesicle exocytosis to cell adhesion in brain. *Cell* **94**, 773–782 (1998).
61. A. Maximov, T. C. Südhof, I. Bezprozvanny, Association of neuronal calcium channels with modular adaptor proteins. *J. Biol. Chem.* **274**, 24453–24456 (1999).
62. W. V. Chen, T. Maniatis, Clustered protocadherins. *Dev. Camb. Engl.* **140**, 3297–3302 (2013).
63. A. Pancho, T. Aerts, M. D. Mitsogiannis, E. Seuntjens, Protocadherins at the crossroad of signaling pathways. *Front. Mol. Neurosci.* **13**, 117 (2020).
64. S. J. Wood, C. R. Slater, Safety factor at the neuromuscular junction. *Prog. Neurobiol.* **64**, 393–429 (2001).
65. C. R. Slater, Pre- and post-synaptic abnormalities associated with impaired neuromuscular transmission in a group of patients with "limb-girdle myasthenia". *Brain* **129**, 2061–2076 (2006).
66. M. M. Rich, H. Colman, J. W. Lichtman, In vivo imaging shows loss of synaptic sites from neuromuscular junctions in a model of myasthenia gravis. *Neurology* **44**, 2138–2138 (1994).
67. J. H. Peragallo, Pediatric myasthenia gravis. *Semin. Pediatr. Neurol.* **24**, 116–121 (2017).
68. A. G. Engel, X.-M. Shen, D. Selcen, S. M. Sine, Congenital myasthenic syndromes: Pathogenesis, diagnosis, and treatment. *Lancet Neurol.* **14**, 420–434 (2015).
69. N. E. Gilhus, J. J. Verschuuren, Myasthenia gravis: Subgroup classification and therapeutic strategies. *Lancet Neurol.* **14**, 1023–1036 (2015).
70. P. Muttathukunnel, P. Frei, S. Perry, D. Dickman, M. Müller, Rapid homeostatic modulation of transsynaptic nanocolumn rings. *Proc. Natl. Acad. Sci. U.S.A.* **119**, e2119044119 (2022).
71. A. DiAntonio, S. A. Petersen, M. Heckmann, C. S. Goodman, Glutamate receptor expression regulates quantal size and quantal content at the drosophila neuromuscular junction. *J. Neurosci.* **19**, 3023–3032 (1999).
72. L. T. Landmesser, Synaptic plasticity: Keeping synapses under control. *Curr. Biol.* **8**, R564–R567 (1998).
73. N. S. Millar, C. Gotti, Diversity of vertebrate nicotinic acetylcholine receptors. *Neuropharmacology* **56**, 237–246 (2009).
74. Y. D. Wang, T. Claudio, Xenopus muscle acetylcholine receptor alpha subunits bind ligands with different affinities. *J. Biol. Chem.* **268**, 18782–18793 (1993).
75. F. M. Lambert *et al.*, Functional limb muscle innervation prior to cholinergic transmitter specification during early metamorphosis in Xenopus. *eLife* **7**, e30693 (2018).
76. W. M. Fu, H. C. Liou, Y. H. Chen, S. M. Wang, Coexistence of glutamate and acetylcholine in the developing motoneurons. *Chin. J. Physiol.* **41**, 127–132 (1998).
77. M. Bertuzzi, W. Chang, K. Ampatzis, Adult spinal motoneurons change their neurotransmitter phenotype to control locomotion. *Proc. Natl. Acad. Sci. U.S.A.* **115**, E9926–E9933 (2018).
78. G. G. Turrigiano, K. R. Leslie, N. S. Desai, L. C. Rutherford, S. B. Nelson, Activity-dependent scaling of quantal amplitude in neocortical neurons. *Nature* **391**, 892–896 (1998).
79. C. C. Steinmetz *et al.*, Upregulation of μ3A drives homeostatic plasticity by rerouting AMPAR into the recycling endosomal pathway. *Cell Rep.* **16**, 2711–2722 (2016).
80. D. A. Wagh *et al.*, Bruchpilot, a protein with homology to ELKS/CAST, is required for structural integrity and function of synaptic active zones in *Drosophila*. *Neuron* **49**, 833–844 (2006).
81. C. A. Frank, M. J. Kennedy, C. P. Goold, K. W. Marek, G. W. Davis, Mechanisms underlying the rapid induction and sustained expression of synaptic homeostasis. *Neuron* **52**, 663–677 (2006).
82. A. Weyhersmuller, S. Hallermann, N. Wagner, J. Eilers, Rapid active zone remodeling during synaptic plasticity. *J. Neurosci.* **31**, 6041–6052 (2011).
83. G. Ouanounou, G. Baux, T. Bal, A novel synaptic plasticity rule explains homeostasis of neuromuscular transmission. *eLife* **5**, e12190 (2016).
84. O. E. Harish, M. Poo, Retrograde modulation at developing neuromuscular synapses: Involvement of G protein and arachidonic acid cascade. *Neuron* **9**, 1201–1209 (1992).
85. H. W. Tao, M. Poo, Retrograde signaling at central synapses. *Proc. Natl. Acad. Sci. U.S.A.* **98**, 11009–11015 (2001).
86. S. K. Jakawich *et al.*, Local presynaptic activity gates homeostatic changes in presynaptic function driven by dendritic bdnf synthesis. *Neuron* **68**, 1143–1158 (2010).
87. A. A. Cole, T. S. Reese, Transsynaptic assemblies link domains of presynaptic and postsynaptic intracellular structures across the synaptic cleft. *J. Neurosci. Off. J. Soc. Neurosci.* **43**, 5883–5892 (2023).
88. C. Gargioli, J. M. W. Slack, Cell lineage tracing during *Xenopus* tail regeneration. *Development* **131**, 2669–2679 (2004).